ACS Energy LETTERS

http://pubs.acs.org/journal/aelccp

LETTER

Understanding the Performance-Limiting Factors of $Cs_2AgBiBr_6$ Double-Perovskite Solar Cells

Giulia Longo,* Suhas Mahesh, Leonardo R. V. Buizza, Adam D. Wright, Alexandra J. Ramadan, Mojtaba Abdi-Jalebi, Pabitra K. Nayak, Laura M. Herz, and Henry J. Snaith*

Cite This: *ACS Energy Lett.* 2020, 5, 2200−2207

Read Online

ACCESS | Metrics & More | Article Recommendations | Supporting Information

ABSTRACT: Double perovskites have recently emerged as possible alternatives to lead-based halide perovskites for photovoltaic applications. In particular, $Cs_2AgBiBr_6$ has been the subject of several studies because of its environmental stability, low toxicity, and its promising optoelectronic features. Despite these encouraging features, the performances of solar cells based on this double perovskite are still low, suggesting severe limitations that need to be addressed. In this work we combine experimental and theoretical studies to show that the short electron diffusion length is one of the major causes for the limited performance of $Cs_2AgBiBr_6$ solar cells. Using EQE measurements on semitransparent $Cs_2AgBiBr_6$ solar cells we estimate the electron diffusion length to be only 30 nm and corroborated this value by terahertz spectroscopy. By using photothermal deflection spectroscopy and surface photovoltage measurements we correlate the limited electron diffusion length with a high density of electron traps. Our findings highlight important faults affecting this double perovskite, showing the challenges to overcome and hinting to a possible path to improve the efficiency of $Cs_2AgBiBr_6$ solar cells.

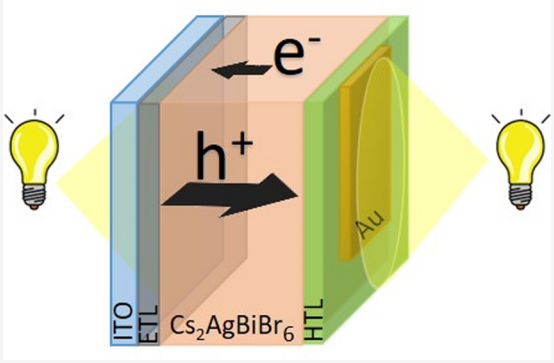

In the past decade, organic−inorganic lead-halide perovskites have been the protagonists of a remarkable ascent in the photovoltaic landscape, with the power conversion efficiency of single-junction solar cells skyrocketing to 25.2% in less than 10 years of investigation and over 29% when integrated into tandem cells with silicon.[1] Despite the impressive photovoltaic performance, these hybrid materials present some drawbacks. In fact, even the best perovskite-based cells currently have much lower operating lifetimes in the ambient (thousands of hours)[2] than traditional inorganic semiconductor-based cells (~25 years). The volatility of the organic cation is considered to be a significant contributor to this instability,[3,4] which should be improved using inorganic cations. However, attempts to utilize the inorganic perovskite $CsPbI_3$ have been thwarted by the intrinsic thermodynamic instability of the photoactive phase at room temperature.[5,6] Additionally, there are some concerns due to the presence of lead, as well as the almost exclusive use of toxic solvents in solution processing. While studies thus far have indicated that the associated risk of the use of lead is small, when deployed in utility scale solar,[2,7,8] social barriers toward the use of lead may need to be addressed.[9] Furthermore, there may simply be other materials which are yet to be discovered, which could have properties superior to those of lead-halide perovskites. For these reasons, the search for alternative inorganic perovskites employing less toxic metals is of high interest. The flexible perovskite crystal structure admits a staggering number of elements with wide variety of configurations[10] and therefore represents an ideal set for conducting this search. The model perovskite should retain the near-ideal optoelectronic properties (long diffusion length, low trap density, and direct band gap ideally between 1 and 1.8 eV).

In this landscape, double perovskites have recently emerged as particularly promising alternatives[11−13] exhibiting encouraging optoelectronic properties, high environmental stability, and low toxicity. In the double-perovskite crystal, Pb^{2+} is replaced

Received: May 11, 2020
Accepted: June 4, 2020
Published: June 4, 2020

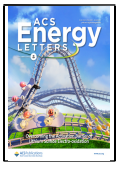

https://dx.doi.org/10.1021/acsenergylett.0c01020
ACS Energy Lett. 2020, 5, 2200−2207

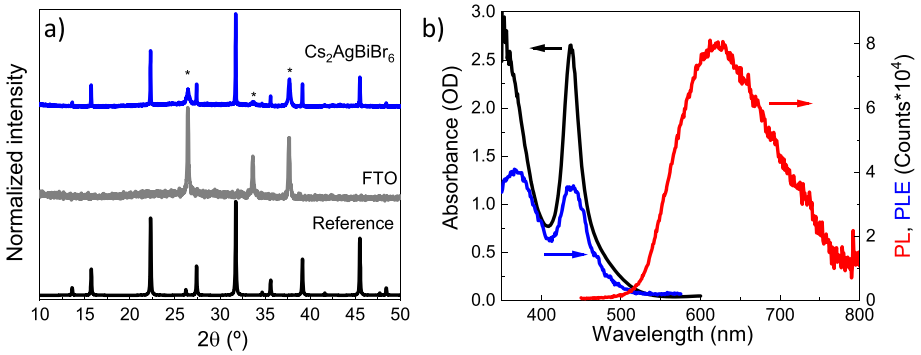

Figure 1. (a) XRD pattern of the evaporated and annealed $Cs_2AgBiBr_6$ thin film on FTO. (b) Absorption (black curve), PL excitation spectrum (PLE, blue curve, recorded at 600 nm emission peak), and PL spectrum (red curve, excitation at 405 nm) of $Cs_2AgBiBr_6$ thin film deposited on quartz.

by alternating monovalent and trivalent metal cations, thus preserving an average divalency. The resulting three-dimensional structure takes the form $A_2M'M''X_6$, where A is a monovalent cation; M′ and M″ are monovalent and trivalent metal ions, respectively; and X is a halide anion. Initial computational studies pointed to pnictogens (Bi^{3+} and Sb^{3+}) and noble metals (Cu^+, Ag^+, and Au^+) as optimal substitutes for Pb^{2+}, because of their stable oxidation states, high conductivity in the metallic form, and ionic radii comparable to that of Pb^{2+} in an octahedral environment.[14,15] Recent works on the $Cs_2M'M''X_6$ family (M′ = Au^+, Ag^+, Cu^+ and M″ = Bi^{3+}, Sb^{3+}) have revealed encouraging optoelectronic properties, characterized by visible to near-infrared absorption,[16−18] relatively small carrier effective mass,[14] and bright emission.[19,20]

In particular, the double-perovskite $Cs_2AgBiBr_6$ has been the subject of much fundamental material characterization and initial application in photodetectors and photovoltaic devices.[11,16,18,21−25] Material characterization and calculations suggest promising features: single-crystal carrier lifetime of 1 μs, moderate charge-carrier mobility, and an absorption-edge in the visible.[26] However, despite these favorable characteristics, the best reported photovoltaic power conversion efficiency (PCE) for a planar heterojunction solar cell is still only 2.84%, with an open-circuit voltage (V_{OC}) of 1.06 V, fill factor (FF) of 0.524, and short-circuit current (J_{SC}) of 5.13 mA cm^{-2}.[25] It is historically common that incipient PV technologies suffer from large voltage deficits, which gradually reduce as material processing improves and as methods to passivate defects are discovered.[27] However, the severely inhibited J_{SC} is unusual and could prove to be a major barrier to high performance. Furthermore, because of the indirect band gap of $Cs_2AgBiBr_6$, thick absorber films, on the order of tens to hundreds of micrometers, would be necessary to substantially increase the photocurrent generation, but this would require extremely long charge-carrier diffusion lengths. For this reason, knowing the charge-carrier mobility and diffusion length is fundamental to choose the proper material thickness for high short-circuit currents. Notwithstanding this, a clear evaluation of these parameters in this material is still missing, and to date, several different values have been reported.[26,28−31]

Here, we undertake a thickness-dependent study of vapor deposited $Cs_2AgBiBr_6$-based solar cells. We evaluate the carrier diffusion length based on the combination of external quantum efficiency (EQE) measurements on semitransparent devices and optical modeling and compare it to values we estimate using terahertz photoconductivity spectroscopy and time-resolved photoluminescence. We specifically reveal that short electron diffusion length, on the order of a few tens of nanometers, is the cause for low short-circuit current densities reported in these solar cells. We also perform photothermal deflection spectroscopy (PDS) and surface photovoltage measurements (SPV) and correlate this short electron diffusion length with the presence of a high density of electron traps. We suggest that the electron diffusion lengths in $Cs_2AgBiBr_6$ must be improved as a matter of priority in order to achieve better performance. Such improvements, likely driven by reduction in trap densities, would also increase open-circuit voltages and reduce hysteresis.

In this work we prepare $Cs_2AgBiBr_6$ thin films through sequential evaporation, as described in the Supporting Information. To assess the successful formation of the double perovskite, we performed X-ray diffraction (XRD) of thin films deposited on FTO. The sharp peaks in the XRD pattern (Figure 1a) of the evaporated material confirm its high crystallinity and the absence of any additional phases or unreacted precursors. Optical properties measured on a quartz substrate [absorbance, photoluminescence (PL) spectra, and photoluminescence excitation (PLE) spectra] are presented in Figure 1b and are consistent with previous reports.[16,32,33] The films exhibit strong and increasing absorption below 400 nm, which has been identified with the direct band gap at ∼3 eV. The strong peak at 440 nm is still subject of controversy: some identify it with a tightly bound exciton at the direct band gap edge,[34,35] whereas others ascribe it to a strong transition between the Bi^{3+} s−p orbitals, without bound character.[36,37] The weak absorption tail beyond 440 nm is considered to be the indirect band gap, which we will return to later. The large Stokes shift between absorption and emission, the similarity between the absorption and PLE spectra, and the independence of the PLE spectra from the emission wavelength at which they are measured (Figure S1) are common signals of charge−lattice interaction mechanisms, like polaron formation, self-trapped excitons, or color-center formations, as previously reported in other works.[20,24,38−40] We note that recently Zelewski et al. observed a "quenching" of the PLE spectra of $Cs_2AgBiBr_6$ single crystals, for excitations around 2.8 eV (440 nm). We cannot observe this same quenching in the thin films here, except for the weak emission detected at wavelengths shorter than 520 nm (Figure S1). It is beyond the scope of our present work to investigate further into this phenomenon, but

https://dx.doi.org/10.1021/acsenergylett.0c01020
ACS Energy Lett. 2020, 5, 2200−2207

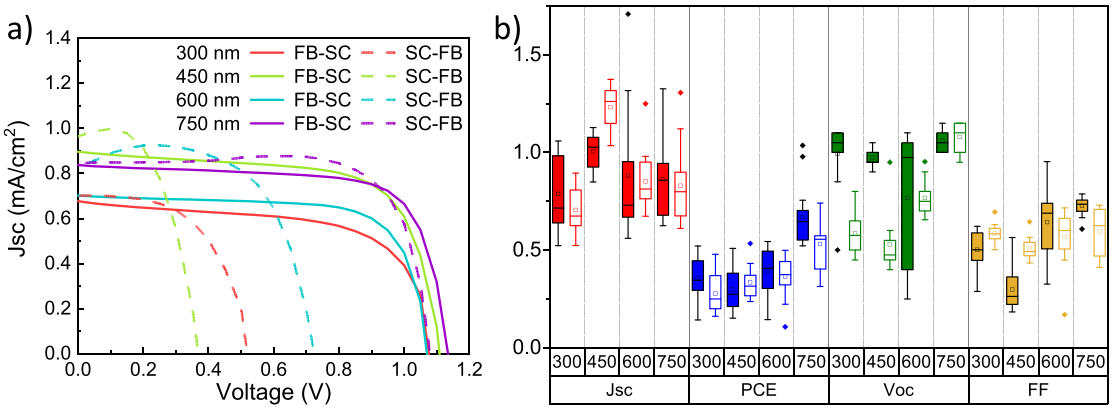

Figure 2. (a) $J-V$ curves of the solar cells with different $Cs_2AgBiBr_6$ thickness. (b) J_{SC} (mA/cm^2, red), PCE (%, blue), V_{OC} (V, green), and FF (yellow) of 15 cells for each $Cs_2AgBiBr_6$ thickness. Forward-bias to short-circuit (FB-SC) scans and data are shown as solid lines and filled bars, and short-circuit to forward-bias (SC-FB) scans and data are shown as dashed lines and open bars.

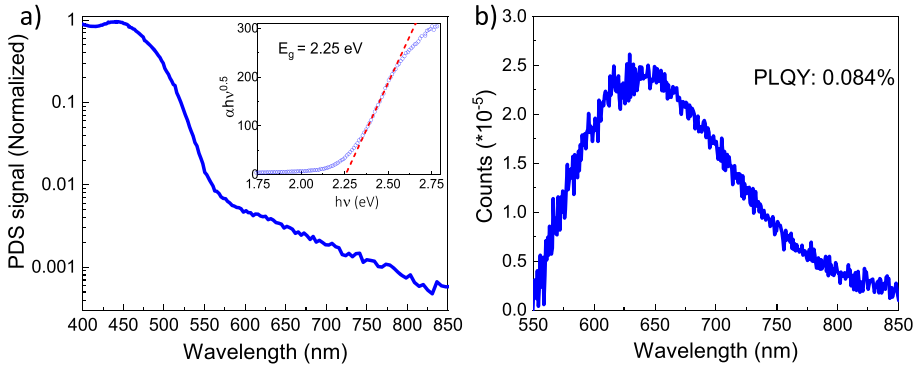

Figure 3. (a) PDS spectrum of neat $Cs_2AgBiBr_6$ film on quartz glass. (Inset) Tauc plot with the calculated indirect band gap reported. (b) PL spectrum and PLQY value of $Cs_2AgBiBr_6$ measured in an integrating sphere with 405 nm laser excitation.

we highlight that ambiguities around the whole nature of photoexcitation and emission in this material still persist.

We then prepared double-perovskite n-i-p cells with different active layer thicknesses. The structure of the fabricated n-i-p cell is FTO/TiO_2/$Cs_2AgBiBr_6$/Spiro-OMeTAD/Ag, as described in the Supporting Information and schematically represented in Figure S2a. In Figure 2a we present the $J-V$ curves of the best devices for each film thickness, while in Figure S2b we present the corresponding steady-state J_{SC} and steady-state power output (SPO) which are similar to those obtained from voltage scans (Table S1). The champion device, obtained with 750 nm of the double-perovskite active layer, was measured to have a PCE of 1.03%, with an open-circuit voltage (V_{OC}) of 1.10 V, short-circuit current (J_{SC}) of 1.33 mA cm^{-2}, and a fill factor (FF) of 0.70, which are comparable to those of previous reports.[41−43] Interestingly, we do not observe any clear trend between the device performance and the active layer thickness, as Figure 2b reveals. We show the XRD patterns of perovskite layers of different thickness in Figure S2c, which exclude the possibility of unwanted phases or unreacted precursors in the different films.

In the inset to Figure 3a, we show a Tauc plot of the absorption spectra, from which we determine an indirect band gap at 2.25 eV, similar to previous reports.[14,16] For such a material, the thermodynamic limit, for the performance (with the Shockley−Queisser assumptions[44]) would be 17.6%, with V_{OC} = 1.93 V and J_{SC} = 9.79 mA cm^{-2}. Every 60 mV loss in V_{OC} from the thermodynamic limit corresponds to an order-of-magnitude reduction in the external radiative efficiency (ERE).[45−47] Our devices exhibit a large voltage deficit of ∼800 mV, suggesting an extremely low external radiative efficiency (ERE) of ∼10^{-13} for a full device with injection condition comparable to 1 sun. In comparison, the best inorganic−organic perovskite cells have ERE ≈ 0.1. This is indicative of an extremely high rate of nonradiative recombination, which in turn indicates extremely large trap densities or other nonradiative processes. We investigate the sub-band gap absorption in these thin films via photothermal deflection optical absorption spectroscopy (PDS, Figure 3a). This observation reveals a shallow absorption edge with an Urbach energy of 70 meV and significant "panchromatic" absorption, at between 1% and 0.1% of the peak absorption strength, reaching down to 1000 nm. This is consistent with a large density of sub-band gap states, which we would expect to mediate fast charge-carrier trapping and subsequent non-radiative recombination. We measured the PL quantum yield (PLQY) of our neat $Cs_2AgBiBr_6$ thin films on glass (Figure 3b), determining a value of ∼0.08% (∼10^{-4}). Although this PLQY value is low, as compared to lead-halide perovskites, it is orders of magnitude higher than the 10^{-13} required to justify such low V_{oc} in the solar cells assuming a Shockley−Queisser type step function absorption spectrum. However, even in the radiative limit, the shallow absorption onset and the presence of such sub-band gap states can be expected to significantly limit the open-circuit voltage in PV devices. This is due to the dark recombination current density (J_0) being proportional to the overlap integral of the blackbody spectrum under ambient

https://dx.doi.org/10.1021/acsenergylett.0c01020
ACS Energy Lett. 2020, 5, 2200−2207

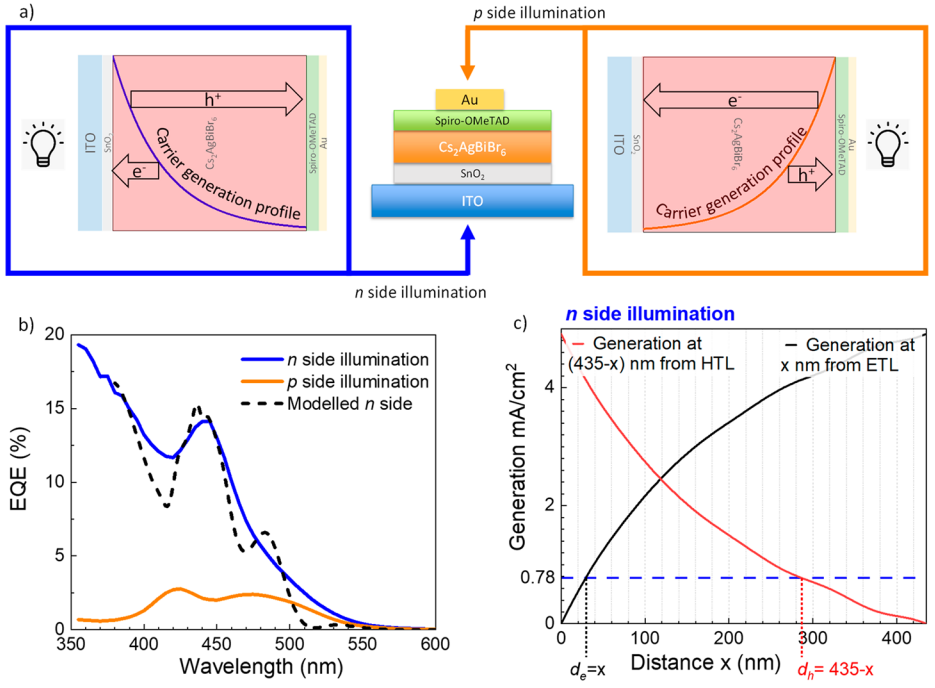

Figure 4. (a) Schematic illustration of the device structure used in the double-side EQE measurement and the two measurement conditions, with the corresponding carrier generation profile. (b) EQE measured with illumination from the ITO (blue curve), from the gold (orange curve), and the modeled n-EQE (black dashed curve). (c) Current generation at a distance x from the ETL (black curve) and from a distance $435 - x$ from the HTL (red curve) in the case of n-side illumination. The dotted blue line indicates the current obtained from the integration of the n-EQE.

temperature (300 K) and the absorption spectrum of the solar absorber material. Because the 300 K blackbody spectrum increases exponentially moving toward lower energy, this factor, J_0, is highly sensitive to small changes in both the steepness of the absorption onset (Urbach energy) and sub-band gap absorptions.[27] Furthermore, charge quenching at the interface between the absorber layer and the charge extraction layer is also usually responsible for significantly quenching the luminescence efficiency in lead-halide perovskite PV cells.[48] This is specifically problematic for wider band gap absorber materials,[47] where there has been little work to date appropriately matching the energetics at these interfaces. Therefore, further improvement in V_{oc} is likely to be feasible via better selection of materials for charge extraction layer or tuning of this interface to minimize recombination losses. Historically, PV technologies started off with hundreds of millielectronvolts of voltage deficit, which slowly improved as materials processing and device architecture design improved. However, the very low photocurrent density, representing a loss of ~90% of the absorbed photons, is not typical, even for incipient materials. Consequently, we must consider the possible origin of these photocurrent losses.

To answer this question, we investigate the charge transport and photocurrent generation in complete $Cs_2AgBiBr_6$ solar cells and thin film in order to estimate the carrier diffusion lengths and reveal if there exists an asymmetry in the electron and hole conduction out of the device. We first fabricated semitransparent PV cells with 435 nm of $Cs_2AgBiBr_6$ and measured their photovoltaic external quantum efficiency (EQE) spectra through front illumination (through the n side), and rear illumination (through the p side), which we schematically represent in Figure 4a. When illuminated through the n side, the EQE (blue curve in Figure 4b) has a peak of ~15%, which very closely matches the absorption spectrum in shape, and has an air-mass (AM) 1.5 integrated current of 0.78 mA cm^{-2}. When illuminated through the p side, the EQE (orange curve in Figure 4b) peaks at only 2.5%, has a shape that counter-correlates with the absorption spectrum, and gives an AM1.5 integrated current of 0.16 mA cm^{-2}. We note that the light attenuation from the 20 nm thick "semi-transparent" gold (~20% at 450 nm) is not sufficient to account for this effect. To understand these results, we have to consider that as light passes through the perovskite, its intensity decays exponentially with depth accordingly to the Beer–Lambert law. This means that the density of generated carriers will be greater closer to the transport layer from which light enters in the device [i.e., greater density next to the electron-transport layer (ETL) for n-side illumination, and greater density close to the hole-transport layer (HTL) for p-side illumination, as represented by the carrier generation profile curves in Figure 4a]. Consequently, with the n-side illumination, holes will have the longer path to travel to be extracted, as compared to electrons, while for p-side illumination electrons will have to travel further than holes to reach the ETL, as indicated by the open arrows in Figure 4a. Considering the EQE in Figure 4b, it is clear that the p-side EQE is much lower than the n-side EQE, indicating that when electrons have to travel across the entire active layer thickness, they cannot be efficiently collected. Furthermore, the p-side EQE also shows an "inversion" in shape in comparison to the n-side EQE and to the absorption spectrum: the peak in the absorption at 440 nm corresponds to a dip in the p-side EQE. This happens because wavelengths that are strongly absorbed do not reach the far end (electron-transporting layer in this case), causing a dip. Weakly absorbed wavelengths, instead, propagate to the far end in greater numbers, appearing as

https://dx.doi.org/10.1021/acsenergylett.0c01020
ACS Energy Lett. 2020, 5, 2200–2207

peaks. In contrast, the *n*-side EQE spectrum very closely follows the absorption spectra, with the clearly defined peak at 440 nm, rather than the total absorptance spectrum, which for this 435 nm thick film is much broader, as we illustrate in Figure S3. This observation is consistent with only a very thin section of the film near the electron extraction layer contributing to photocurrent generation.

These considerations lead us to conclude that electron diffusion is the factor limiting the short-circuit current of $Cs_2AgBiBr_6$ solar cells. We then combined our EQE data with an optical model (generalized transfer matrix method) to obtain a quantitative estimation of the electron and hole diffusion length in our devices (Figure 4c). For this, we made the following simplified consideration: if the diffusion length of electrons is d_e, we assume that only electrons generated within a length d_e from the ETL will be collected. We make the same assumption for the diffusion length of holes d_h, and undertake that the overall short-circuit current in the device will be governed by the smaller of the electron and hole currents. We then modeled the carrier generation profile as a function of incident light wavelength using the generalized transfer matrix method and estimated the total light absorbed as a function of wavelength within a length d of a transport layer. This allowed us to reconstruct the contribution to the EQE spectrum, for every section of film with thickness d, with the assumption of an abrupt interface at d; all light absorbed within d is converted to collected photocurrent, while all light absorbed beyond d is lost. Additionally, we assume that the solar cell current is limited by the smaller of the electron and hole currents. Assuming *n*-side illumination, we varied d until the modeled EQE best approximated the measured spectrum, which we show in Figure 4b,c. This tells us that under these assumptions, the electron diffusion length d_e is ∼30 nm and that the hole diffusion length d_h > 150 nm (note greater than, not approximately). We executed the same procedure for the *p*-side illumination (Figure S4). However, we remark that the unavailability of the optical constants of the thin gold semitransparent electrode causes an underestimation in the EQE modeled for *p*-side illumination. We also note that the interference fringes visible in our modeled EQE spectrum (Figure 4b), which are not replicated in the experimental data, are likely to reflect that the physical material interfaces are not perfectly smooth in the real devices, as required for coherent optical interference.

To further investigate charge-carrier mobility, and to corroborate the above estimated carrier diffusion lengths ($d_e \approx 30$ nm, $d_h > 150$ nm), we performed optical-pump−terahertz-probe (OPTP) photoconductivity measurements (see the Supporting Information for a more exhaustive explanation).[28,41,49,50]

We report the results in Figure S5a. Our OPTP measurements give a sum mobility of $\phi\Sigma\mu = 0.74 \pm 0.29$ cm^2 V^{-1} s^{-1}, in good agreement with previous measurements carried out by time-resolved microwave conductivity.[28] From the measured mobility we obtained the charge-carrier diffusion length by calculating the diffusion coefficient and knowing the recombination rate, as described in the Supporting Information. To estimate the recombination rate, we performed time-correlated single-photon counting (TCSPC), and we present the time-resolved PL decay in Figure S5b. The highly heterogeneous nature of the PL decay has been previously reported, both in thin films and single crystals.[28,34] Fitting the PL decay using a monoexponential and a stretched exponential function we obtained values for k_1 of 5−38.5 × 10^7 s^{-1} (see the Supporting Information for the discussion on the evaluation of k_1). Approximating $R_T(n) \approx k_1$, we calculate values of 70−200 nm for the diffusion length. Although THz photoconductivity measurements cannot distinguish between electron and hole contributions to the charge-carrier mobility, providing a sum mobility, these diffusion lengths are in reasonably close agreement with the values obtained from our EQE model above. Alternatively, this mobility estimated by THz spectroscopy is also likely to represent an upper estimate of the long-range mobility in the solar cell devices, where for the latter charge conduction is sensitive to scattering events on longer length scales.

The presence of traps states, especially at the surface and at interfaces with the extraction layers, is a common reason for short carrier lifetimes in semiconductor devices. So far we presented consistent evidence of the presence of a significant density of traps in $Cs_2AgBiBr_6$. In order to gain a deeper understanding on the nature of these trap states, we performed Kelvin probe surface photovoltage (SPV) measurements on a double-perovskite thin film deposited on top of the FTO substrates and on different transport layers. Kelvin probe is a noninvasive technique that permits evaluating the work function of the material of interest through capacitance measurements between the sample and an oscillating tip with known work function. A detailed working mechanism of this technique is reported in the Supporting Information and in Figure S6. We determine the work function of the $Cs_2AgBiBr_6$ thin film deposited on FTO, measured in dark and nitrogen atmosphere, to be 4.91 eV, which is very close to the value of 4.94 eV that we obtained from ultraviolet photoelectron spectroscopy (UPS) measurements, which were conducted under ultrahigh vacuum and are presented in Figure S7. Interestingly, from UPS, we determined a deep-lying valence band maximum (VBM) at around 6.8 ± 0.3 eV (see the Supporting Information for further discussion and discussion on error margins). Knowing that the optical band gap is ∼2.25 eV and assuming a negligible exciton binding energy, this indicates that we expect the position of the conduction band minimum (CBM) to be at ∼ 4.55 eV. Therefore, the position of the Fermi level (analogous to the work function in the KP measurements) would appear closer to the CBM, suggesting that our sequentially evaporated $Cs_2AgBiBr_6$ thin film is n-type in nature. Our result here contrasts with the previously reported works, in which this double perovskite was presented as p-type semiconductor,[26,51,52] and also seems to be counterintuitive to our estimation of very short electron diffusion lengths, because electrons should be the majority carrier in our "n-type" material. However, it is known that defect formation (and consequently the majority carrier population) are strongly influenced by the material fabrication technique that can substantially alter the semiconductor electronic properties.[53] Our results indicate that sequentially evaporated $Cs_2AgBiBr_6$ thin films present an n-type character, possibly related to Br^- vacancies,[31] as has been previously inferred.[24] However, we also note that UPS measurements probe the electronic structure of the utmost surface of a sample. Therefore, the presence of defects on the surface could account for the discrepancies between our measurements and previous reports.

We present surface photovoltage (SPV) measurements of the double-perovskite films on FTO and on different transport layers in panels a and b of Figure 5, respectively.

https://dx.doi.org/10.1021/acsenergylett.0c01020
ACS Energy Lett. 2020, 5, 2200−2207

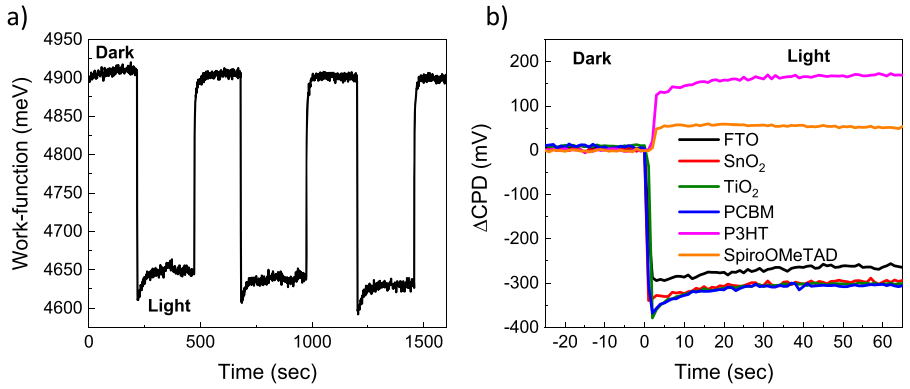

Figure 5. (a) Work function of a $Cs_2AgBiBr_6$ thin film on FTO in the dark and under white light. (b) Contact potential difference of a $Cs_2AgBiBr_6$ thin film on different charge carrier transport materials.

SPV measures the change of the contact potential difference (CPD) between the sample surface and the Kelvin probe tip when the sample is illuminated and it is defined as SPV = $CPD_{light} - CPD_{dark}$.[54] Observing the direction of the potential bending and its change with illumination, it is possible to gather information about the nature of the surface states of the semiconductor material investigated. In Figure 5a the SPV of the evaporated double perovskite on FTO is reported. Under illumination, the work function decreases, generating an SPV of almost −250 mV. Considering the n-type character of the material, a negative SPV indicates a reduction of the band bending (see Figure S6e), consistent with the presence of electron traps. Interestingly, we observe that under illumination, the CPD (and, consequently, the calculated work function) has an unsteady behavior, flattening after several seconds of light exposure. The long time scale necessary for its stabilizations suggests that this phenomenon is due or influenced by a slow process, likely ionic movement. However, this behavior is fully recoverable, because the dark work-function value is the same even after several cycles of illumination.

Finally, we evaluate the SPV of the double perovskite on different hole and electron transport layers (Figure 5b). All the CPD_{dark} values where set to 0 mV, in order to facilitate the comparison between the different samples. When the double perovskite is deposited on top of electron transport materials (as SnO_2, TiO_2, or PCBM), the SPV value becomes slightly more negative than on FTO, reaching values of −300 mV. This can be understoodby considering that as the free carriers are created under illumination, the electrons are selectively extracted by the transport material at the buried interface, leaving a higher hole concentration than on FTO. The remaining holes annihilate the trapped electron at the surface, decreasing even more the band bending. In contrast, when a hole transport material is used as an underlying layer (as Spiro or P3HT), the SPV becomes positive (+50 mV and +150 mV, respectively). After photogeneration, holes get mostly extracted by the hole transport layer while electrons remain in the double-perovskite film, increasing the surface band bending, then creating a positive SPV. These results are hence also consistent with the presence of electron traps at the double-perovskite surface, indicating a prevalence of electron trapping in this material.

In summary, in this work, through a combined experimental and theoretical study, we have obtained a deeper understanding of the limiting factor for the performance of $Cs_2AgBiBr_6$ solar cells. A thickness-dependent study of the photovoltaic parameters of the double-perovskite devices revealed that the J_{SC} is independent of the absorber thickness but much lower than expected from the total light absorbed in the films. We resolved these apparent contradictory results by analyzing the EQE spectrum via illumination through the front and back sides of the cells and revealed that the material suffers from a very low electron diffusion length but has a substantial hole-diffusion length. This observation is corroborated using THz spectroscopy, from which we determined a modest sum mobility of electrons and holes of less than 1 $cm^2 V^{-1} s^{-1}$ and a corresponding charge carrier diffusion length of between 70 to 200 nm. We ascribe this short electron diffusion length to the presence of energetic disorder and specifically a high density of electron traps, which we revealed by PDS measurements and surface photovoltage analysis. We believe that these results represent a significant step forward for understanding the deficiencies of double perovskites for photovoltaic applications and hence elucidate the next challenges which need to be addressed in order to improve the performance of this promising class of double-perovskite materials and optoelectronic devices.

■ ASSOCIATED CONTENT

Supporting Information

The Supporting Information is available free of charge at https://pubs.acs.org/doi/10.1021/acsenergylett.0c01020.

Experimental section and detailed description of the technique employed in this work; additional graphics and tables (PDF)

■ AUTHOR INFORMATION

Corresponding Authors

Giulia Longo − *Department of Mathematics, Physics and Electrical Engineering, Northumbria University, Newcastle upon Tyne NE18ST, United Kingdom; Clarendon Laboratory, Department of Physics, University of Oxford, Oxford OX13PU, United Kingdom;* orcid.org/0000-0002-1163-1110; Email: g.longo@northumbria.ac.uk

Henry J. Snaith − *Clarendon Laboratory, Department of Physics, University of Oxford, Oxford OX13PU, United Kingdom;* orcid.org/0000-0001-8511-790X; Email: henry.snaith@physics.ox.ac.uk

https://dx.doi.org/10.1021/acsenergylett.0c01020
ACS Energy Lett. 2020, 5, 2200−2207

Authors

Suhas Mahesh − *Clarendon Laboratory, Department of Physics, University of Oxford, Oxford OX13PU, United Kingdom*

Leonardo R. V. Buizza − *Clarendon Laboratory, Department of Physics, University of Oxford, Oxford OX13PU, United Kingdom*

Adam D. Wright − *Clarendon Laboratory, Department of Physics, University of Oxford, Oxford OX13PU, United Kingdom;* orcid.org/0000-0003-0721-7854

Alexandra J. Ramadan − *Clarendon Laboratory, Department of Physics, University of Oxford, Oxford OX13PU, United Kingdom;* orcid.org/0000-0003-4572-3459

Mojtaba Abdi-Jalebi − *Institute for Material Discovery, University College London, London WC1E 7JE, United Kingdom; Cavendish Laboratory, Department of Physics, University of Cambridge, Cambridge CB3 0HE, United Kingdom;* orcid.org/0000-0002-9430-6371

Pabitra K. Nayak − *TIFR Centre for Interdisciplinary Sciences, Tata Institute of Fundamental Research, Hyderabad 500107, India*

Laura M. Herz − *Clarendon Laboratory, Department of Physics, University of Oxford, Oxford OX13PU, United Kingdom;* orcid.org/0000-0001-9621-334X

Complete contact information is available at: https://pubs.acs.org/10.1021/acsenergylett.0c01020

Notes

The authors declare no competing financial interest.

■ ACKNOWLEDGMENTS

This work was funded by EPSRC through projects EP/M015254/2, EP/S516119/1, EP/M005143/1, and EP/P032591/1 and by H2020 through the European Union's Horizon 2020 research and innovation programme through PERTPV project under Grant Agreement No. 763977 and CHEOPS project under Grant Agreement No. 730135. S.M. acknowledges funding from the Rhodes Trust (India & Worcester 2016). L.R.V.B. thanks the Centre for Doctoral Training in New and Sustainable Photovoltaics and to the Oxford-Radcliffe Scholarship for financial support. P.K.N. acknowledges the support via intramural funds at TIFR Hyderabad from the Department of Atomic Energy (DAE), India. M.A.-J. thanks Cambridge Materials Limited, Wolfson College, University of Cambridge, and EPSRC for their funding and technical support.

■ REFERENCES

(1) NREL. Best Research-Cell Efficiencies, https://www.nrel.gov/pv/cell-efficiency.html (2020).

(2) Meng, L.; You, J.; Yang, Y. Addressing the stability issue of perovskite solar cells for commercial applications. *Nat. Commun.* **2018**, *9*, 5265.

(3) Zhou, Y.; Zhao, Y. Chemical stability and instability of inorganic halide perovskites. *Energy Environ. Sci.* **2019**, *12*, 1495−1511.

(4) Park, B.-w.; Seok, S. I. Intrinsic Instability of Inorganic−Organic Hybrid Halide Perovskite Materials. *Adv. Mater.* **2019**, *31*, 1805337.

(5) Eperon, G. E.; Paternò, G. M.; Sutton, R. J.; Zampetti, A.; Haghighirad, A. A.; Cacialli, F.; Snaith, H. J. Inorganic caesium lead iodide perovskite solar cells. *J. Mater. Chem. A* **2015**, *3*, 19688−19695.

(6) Sharma, S.; Weiden, N.; Weiss, A. *Z. Phys. Chem.* **1992**, *175*, 63.

(7) Babayigit, A.; Ethirajan, A.; Muller, M.; Conings, B. Toxicity of organometal halide perovskite solar cells. *Nat. Mater.* **2016**, *15*, 247−251.

(8) CHEOPS EU Project, D3.1: Life Cycle Analysisof CHEOPS technologies and benchmarking: Screening, https://www.cheops-project.eu/reports/ (2017).

(9) CHEOPS EU Project, D3.4: Socio-economic analysis of CHEOPS technologies and benchmarking, https://www.cheops-project.eu/reports/ (2019).

(10) Filip, M. R.; Giustino, F. The geometric blueprint of perovskites. *Proc. Natl. Acad. Sci. U. S. A.* **2018**, *115*, 5397−5402.

(11) Shi, Z.; Guo, J.; Chen, Y.; Li, Q.; Pan, Y.; Zhang, H.; Xia, Y.; Huang, W. Lead-Free Organic−Inorganic Hybrid Perovskites for Photovoltaic Applications: Recent Advances and Perspectives. *Adv. Mater.* **2017**, *29*, 1605005.

(12) Fu, H. Review of lead-free halide perovskites as light-absorbers for photovoltaic applications: From materials to solar cells. *Sol. Energy Mater. Sol. Cells* **2019**, *193*, 107−132.

(13) Chu, L.; Ahmad, W.; Liu, W.; Yang, J.; Zhang, R.; Sun, Y.; Yang, J.; Li, X. Lead-Free Halide Double Perovskite Materials: A New Superstar Toward Green and Stable Optoelectronic Applications. *Nano-Micro Lett.* **2019**, *11*, 16−34.

(14) Volonakis, G.; Filip, M. R.; Haghighirad, A. A.; Sakai, N.; Wenger, B.; Snaith, H. J.; Giustino, F. Lead-Free Halide Double Perovskites via Heterovalent Substitution of Noble Metals. *J. Phys. Chem. Lett.* **2016**, *7*, 1254−1259.

(15) Deng, Z.; Wei, F.; Sun, S.; Kieslich, G.; Cheetham, A. K.; Bristowe, P. D. Exploring the properties of lead-free hybrid double perovskites using a combined computational- experimental approach. *J. Mater. Chem. A* **2016**, *4*, 12025−12029.

(16) McClure, E. T.; Ball, M. R.; Windl, W.; Woodward, P. M. Cs_2AgBiX_6 (X = Br, Cl): New Visible Light Absorbing, Lead-Free Halide Perovskite Semiconductors. *Chem. Mater.* **2016**, *28*, 1348−1354.

(17) Filip, M. R.; Hillman, S.; Haghighirad, A. A.; Snaith, H. J.; Giustino, F. Band Gaps of the Lead-Free Halide Double Perovskites $Cs_2BiAgCl_6$ and $Cs_2BiAgBr_6$ from Theory and Experiment. *J. Phys. Chem. Lett.* **2016**, *7*, 2579−2585.

(18) Slavney, A. H.; Hu, T.; Lindenberg, A. M.; Karunadasa, H. I. A Bismuth-Halide Double Perovskite with Long Carrier Recombination Lifetime for Photovoltaic Applications. *J. Am. Chem. Soc.* **2016**, *138*, 2138−2141.

(19) Volonakis, G.; Haghighirad, A. A.; Milot, R.; Sio, W. H.; Filip, M. R.; Wenger, B.; Johnston, M. B.; Herz, L. M.; Snaith, H. J.; Giustino, F. $Cs_2InAgCl_6$: A New Lead-Free Halide Double Perovskite with Direct Band Gap. *J. Phys. Chem. Lett.* **2017**, *8*, 772−778.

(20) Luo, J.; Wang, X.; Li, S.; Liu, J.; Guo, Y.; Niu, G.; Yao, L.; Fu, Y.; Gao, L.; Dong, Q.; Zhao, C.; Leng, M.; Ma, F.; Liang, W.; Wang, L.; Jin, S.; Han, J.; Zhang, L.; Etheridge, J.; Wang, J.; Yan, Y.; Sargent, E. H.; Tang, J. Efficient and stable emission of warm-white light from lead-free halide double perovskites. *Nature* **2018**, *563*, 541−545.

(21) Wu, C.; Du, B.; Luo, W.; Liu, Y.; Li, T.; Wang, D.; Guo, X.; Ting, H.; Fang, Z.; Wang, S.; Chen, Z.; Chen, Y.; Xiao, L. Highly Efficient and Stable Self-Powered Ultraviolet and Deep-Blue Photodetector Based on $Cs_2AgBiBr_6/SnO_2$ Heterojunction. *Adv. Opt. Mater.* **2018**, *6*, 1800811.

(22) Gao, W.; Ran, C.; Xi, J.; Jiao, B.; Zhang, W.; Wu, M.; Hou, X.; Wu, Z. High-Quality $Cs_2AgBiBr_6$ Double Perovskite Film for Lead-Free Inverted Planar Heterojunction Solar Cells with 2.2% Efficiency. *ChemPhysChem* **2018**, *19*, 1696−1700.

(23) Pan, W.; Wu, H.; Luo, J.; Deng, Z.; Ge, C.; Chen, C.; Jiang, X.; Yin, W.-J.; Niu, G.; Zhu, L.; Yin, L.; Zhou, Y.; Xie, Q.; Ke, X.; et al. $Cs_2AgBiBr_6$ single-crystal X-ray detectors with a low detection limit. *Nat. Photonics* **2017**, *11*, 726.

(24) Igbari, F.; Wang, R.; Wang, Z.-K.; Ma, X.-J.; Wang, Q.; Wang, K.-L.; Zhang, Y.; Liao, L.-S.; Yang, Y. Composition Stoichiometry of $Cs_2AgBiBr_6$ Films for Highly Efficient Lead-Free Perovskite Solar Cells. *Nano Lett.* **2019**, *19*, 2066−2073.

(25) Yang, X.; Yang, X.; Chen, Y.; Liu, P.; Xiang, H.; Wang, W.; Ran, R.; Zhou, W.; Shao, Z. Simultaneous Power Conversion Efficiency and Stability Enhancement of $Cs_2AgBiBr_6$ Lead-Free Inorganic

Perovskite Solar Cell through Adopting a Multifunctional Dye Interlayer. *Adv. Funct. Mater.* **2020**, *30*, 2001557.
(26) Hoye, R. L. Z.; Eyre, L.; Wei, F.; Brivio, F.; Sadhanala, A.; Sun, S.; Li, W.; Zhang, K. H. L.; MacManus-Driscoll, J. L.; Bristowe, P. D.; Friend, R. H.; Cheetham, A. K.; Deschler, F. Fundamental Carrier Lifetime Exceeding 1 μs in $Cs_2AgBiBr_6$ Double Perovskite. *Adv. Mater. Interfaces* **2018**, *5*, 1800464.
(27) Nayak, P. K.; Mahesh, S.; Snaith, H. J.; Cahen, D. Photovoltaic solar cell technologies: analysing the state of the art. *Nat. Rev. Mater.* **2019**, *4*, 269−285.
(28) Bartesaghi, D.; Slavney, A. H.; Gélvez-Rueda, M. C.; Connor, B. A.; Grozema, F. C.; Karunadasa, H. I.; Savenije, T. J. Charge Carrier Dynamics in $Cs_2AgBiBr_6$ Double Perovskite. *J. Phys. Chem. C* **2018**, *122*, 4809−4816.
(29) Hutter, E. M.; Gélvez-Rueda, M. C.; Bartesaghi, D.; Grozema, F. C.; Savenije, T. J. Band-Like Charge Transport in $Cs_2AgBiBr_6$ and Mixed Antimony-Bismuth $Cs_2AgBi_{1-x}Sb_xBr_6$ Halide Double Perovskites. *ACS Omega* **2018**, *3*, 11655−11662.
(30) Dang, Y.; Tong, G.; Song, W.; Liu, Z.; Qiu, L.; Ono, L. K.; Qi, Y. Interface Engineering Strategies Towards $Cs_2AgBiBr_6$ Single-Crystalline Photodetectors with Good Ohmic Contact Behaviours. *J. Mater. Chem. C* **2020**, *8*, 276−284.
(31) Delor, M.; Slavney, A. H.; Wolf, N. R.; Filip, M. R.; Neaton, J. B.; Karunadasa, H. I.; Ginsberg, N. S. Carrier Diffusion Lengths Exceeding 1 μm Despite Trap-Limited Transport in Halide Double Perovskites. *ACS Energy Lett.* **2020**, *5*, 1337−1345.
(32) Gray, M. B.; McClure, E. T.; Woodward, P. M. $Cs_2AgBiBr_{6-x}Cl_x$ Solid Solutions − Band Gap Engineering With Halide Double Perovskites. *J. Mater. Chem. C* **2019**, *7*, 9686.
(33) Schmitz, A.; Leander Schaberg, L.; Sirotinskaya, S.; Pantaler, M.; Lupascu, D. C.; Benson, N.; Bacher, G. Fine Structure of the Optical Absorption Resonance in $Cs_2AgBiBr_6$ Double Perovskite Thin Films. *ACS Energy Lett.* **2020**, *5*, 559−565.
(34) Kentsch, R.; Scholz, M.; Horn, J.; Schlettwein, D.; Oum, K.; Lenzer, T. Exciton Dynamics and Electron-Phonon Coupling Affect the Photovoltaic Performance of the $Cs_2AgBiBr_6$ Double Perovskite. *J. Phys. Chem. C* **2018**, *122*, 25940−25947.
(35) Bass, K. K.; Estergreen, L.; Savory, C. N.; Buckeridge, J.; Scanlon, D. O.; Djurovich, P. I.; Bradforth, S. E.; Thompson, M. E.; Melot, B. C. Vibronic Structure in Room Temperature Photoluminescence of the Halide Perovskite $Cs_3Bi_2Br_9$. *Inorg. Chem.* **2017**, *56*, 42−45.
(36) Bekenstein, Y.; Dahl, J. C.; Huang, J.; Osowiecki, W. T.; Swabeck, J. K.; Chan, E. M.; Yang, P.; Alivisatos, A. P. The Making and Breaking of Lead-Free Double Perovskite Nanocrystals of Cesium Silver-Bismuth Halide Compositions. *Nano Lett.* **2018**, *18*, 3502−3508.
(37) Oldenburg, K.; Vogler, A. Electronic Spectra and Photochemistry of Tin (II), Lead (II), Antimony (III), and Bismuth (III) Bromide Complexes in Solution. *Z. Naturforsch., B: J. Chem. Sci.* **1993**, *48b*, 1519−1523.
(38) McCall, K. M.; Stoumpos, C. C.; Kostina, S. S.; Kanatzidis, M. G.; Wessels, B. W. Strong Electron-Phonon Coupling and Self-Trapped Excitons in the Defect Halide Perovskites $A_3M_2I_9$ (A = Cs, Rb; M = Bi, Sb). *Chem. Mater.* **2017**, *29*, 4129−4145.
(39) Smith, M. D.; Karunadasa, H. I. White-Light Emission from Layered Halide Perovskites. *Acc. Chem. Res.* **2018**, *51*, 619−627.
(40) Steele, J. A.; Puech, P.; Keshavarz, M.; Yang, R.; Banerjee, S.; Debroye, E.; Kim, C. W.; Yuan, H.; Heo, N. H.; Vanacken, J.; Walsh, A.; Hofkens, J.; Roeffaers, M. B. J. Giant Electron-Phonon Coupling and Deep Conduction Band Resonance in Metal Halide Double Perovskite. *ACS Nano* **2018**, *12*, 8081−8090.
(41) Ning, W.; Wang, F.; Wu, B.; Lu, J.; Yan, Z.; Liu, X.; Tao, Y.; Liu, J.-M.; Huang, W.; Fahlman, M.; Hultman, L.; Sum, T. C.; Gao, F. Long Electron-Hole Diffusion Length in High-Quality Lead-Free Double Perovskite Films. *Adv. Mater.* **2018**, *30*, 1706246.
(42) Gao, W.; Ran, C.; Xi, J.; Jiao, B.; Zhang, W.; Wu, M.; Hou, X.; Wu, Z. High Quality $Cs_2AgBiBr_6$ Double Perovskite Film for Lead-Free Inverted Planar Heterojunction Solar Cells with 2.2% Efficiency. *ChemPhysChem* **2018**, *19*, 1696−1701.
(43) Wang, M.; Zeng, P.; Bai, S.; Gu, J.; Li, F.; Yang, Z.; Liu, M. High-Quality Sequential-Vapor-Deposited $Cs_2AgBiBr_6$ Thin Films for Lead-Free Perovskite Solar Cells. *Solar RRL* **2018**, *2*, 1800217.
(44) Shockley, W.; Queisser, H. J. Detailed Balance Limit of Efficiency of p-n Junction Solar Cells. *J. Appl. Phys.* **1961**, *32*, 510−519.
(45) Kirchartz, T.; Rau, U. Detailed balance and reciprocity in solar cells. *Phys. Status Solidi A* **2008**, *205*, 2737−2751.
(46) Liu, Z.; Krückemeier, L.; Krogmeier, B.; Klingebiel, B.; Márquez, J. A.; Levcenko, S.; Öz, S.; Mathur, S.; Rau, U.; Unold, T.; Kirchartz, T. Open-Circuit Voltages Exceeding 1.26 V in Planar Methylammonium Lead Iodide Perovskite Solar Cells. *ACS Energy Lett.* **2019**, *4*, 110−117.
(47) Mahesh, S.; Ball, J. M.; Oliver, R. D. J.; McMeekin, D. P.; Nayak, P. K.; Johnston, M. B.; Snaith, H. J. Revealing the origin of voltage loss in mixed-halide perovskite solar cells. *Energy Environ. Sci.* **2020**, *13*, 258−267.
(48) Stolterfoht, M.; Wolff, C. M.; Márquez, J. A.; Zhang, S.; Hages, C. J.; Rothhardt, D.; Albrecht, S.; Burn, P. L.; Meredith, P.; Unold, T.; Neher, D. Visualization and suppression of interfacial recombination for high-efficiency large-area pin perovskite solar cells. *Nat. Energy* **2018**, *3*, 847−854.
(49) Wehrenfennig, C.; Liu, M.; Snaith, H. J.; Johnston, M. B.; Herz, L. M. Charge-carrier dynamics in vapour-deposited films of the organolead halide perovskite $CH_3NH_3PbI_{3-x}Cl_x$. *Energy Environ. Sci.* **2014**, *7*, 2269−2275.
(50) Johnston, M. B.; Herz, L. M. Hybrid Perovskites for Photovoltaics: Charge-Carrier Recombination, Diffusion, and Radiative Efficiencies. *Acc. Chem. Res.* **2016**, *49*, 146−154.
(51) Xiao, Z.; Meng, W.; Wang, J.; Yan, Y. Thermodynamic Stability and Defect Chemistry of Bismuth-Based Lead-Free Double Perovskites. *ChemSusChem* **2016**, *9*, 2628−2633.
(52) Zhang, Z.; Yang, G.; Zhou, C.; Chung, C. C.; Hany, I. Optical and electrical properties of all-inorganic $Cs_2AgBiBr_6$ double perovskite single crystals. *RSC Adv.* **2019**, *9*, 23459−23464.
(53) Hobson, T. D. C.; Phillips, L. J.; Hutter, O. S.; Shiel, H.; Swallow, J. E. N.; Savory, C. N.; Nayak, P. K.; Mariotti, S.; Das, B.; Bowen, L.; Jones, L. A. H.; Featherstone, T. J.; Smiles, M. J.; Farnworth, M. A.; Zoppi, G.; Thakur, P. K.; Lee, T.; Snaith, H. J.; Leighton, C.; Scanlon, D. O.; Dhanak, V. R.; Durose, K.; Veal, T. D.; Major, J. D. Isotype heterojunction solar cells using n-type Sb_2Se_3 thin films. *Chem. Mater.* **2020**, *32*, 2621−2630.
(54) Cavalcoli, D.; Cavallini, A. Surface photovoltage spectroscopy - method and applications. *Phys. Status Solidi C* **2010**, *7*, 1293−1300.

https://dx.doi.org/10.1021/acsenergylett.0c01020
ACS Energy Lett. 2020, 5, 2200−2207